For submission as an *Article* to *J. Am. Chem. Soc.*

Copper-Linked Rotaxanes for the Building of Photoresponsive Metal Organic Frameworks with Controlled Cargo Delivery

Adrian Saura-Sanmartin,[†] Alberto Martinez-Cuezva,[†] Delia Bautista, [‡] Mara R. B . Marzari ,[§] Marcos A. P. Martins, [§] Mateo Alajarin, [†] Jose Berna[*,†]

[†] Departamento de Química Orgánica, Facultad de Química, Regional Campus of International Excellence "Campus Mare Nostrum", Universidad de Murcia, E-30100 Murcia (Spain). [‡] Sección Universitaria de Instrumentación Científica (SUIC), Área Científica y Técnica de Investigación (ACTI), Universidad de Murcia, E-30100 Murcia (Spain). [§] Núcleo de Química de Heterociclos (NUQUIMHE), Departamento de Química, Universidad Federal de Santa Maria, 97105-900 Santa María-RS (Brazil).

E-mail: ppberna@um.es

RECEIVED DATE (to be automatically inserted after your manuscript is accepted)

Abstract. We have prepared a photoresponsive metal-organic framework by using an amide-based [2]rotaxane as linker and copper(II) ions as metal nodes. The interlocked linker was obtained by the hydrogen bond-directed approach employing a fumaramide thread as template of the macrocyclic component, this latter incorporating two carboxyl groups. Single crystal X-ray diffraction analysis of the metal-organic framework, prepared under solvothermal conditions, showed the formation of stacked 2D rhombohedral grids forming channels decorated with the interlocked alkenyl threads. A series of metal-organic frameworks differing in the *E/Z* olefin ratio were prepared either by the previous isomerization of the linker or by post-irradiation of the reticulated materials. By dynamic solid state ^{2}H NMR measurements, using deuterium-labelled materials, we proved that the geometry of the olefinic axis of the interlocked struts determined the obtention of materials with different independent local dynamics as a result of the strength of the intercomponent non-covalent interactions. Moreover, the usefulness of these novel copper-rotaxane materials as molecular dosing containers has also been assayed by the diffusion and photorelease of *p*-benzoquinone, evaluated in different solvents and temperatures.

Introduction

One of the main strategies for conducting novel investigations on metal organic frameworks (MOFs),[1-9] crystalline materials consisting in organic ligands connected by metal nodes, is focused on the incorporation of advanced level of complexity as an approach to find materials with improved functionalities.[10-13] During the last decades this purpose ran parallel to the development of mechanically interlocked compound-based molecular machines[14-29] and to the inherent need in the field of achieving ordered arrangements in the solid state.[13,30-33] The merging of both topics gave birth to metal organic materials integrating a variety of mechanically interlocked compounds,[34-41] mainly rotaxanes.[37-41] Since the pioneering contributions by using these latter species due to Kim,[42-44] important advances have been made related to the structure and organization of the interlocked ligands into three-dimensional arrays.[13,18] Thus, relevant breakthroughs by Loeb's group focused on the characterization of large amplitude motions, both rotational[45,46] and translational,[47,48] of the crown-ether ring of the rotaxanes by using variable temperature and ^{2}H solid state NMR spectroscopy.[49] The number of contributions studying the control of the ring motion in the solid state is scarce. Although some stimulating examples have been reported, including temperature variation,[46] phase change[50] or the application of a redox stimuli,[51,52] the use of light as the source of control remains unexplored.

In this work, we describe the building of photoresponsive MOFs[53] using benzylic amide [2]rotaxanes[54-65] as organic linkers and copper(II) ions as metal nodes. In addition, their behaviour in the uptake and release of an small guest was also explored.[66-70] In contrast with most of the described coordinating polymers incorporating rotaxanes as linkers, in which the linear interlocked component acts as connector of the metal units, herein we have employed a different approach.[71] In this case we used threaded benzyl amide macrocycles bearing a carboxylic acid group at each isophthalamide unit as connectors of the metal nodes. Although the former approach, consisting in linking threads, somehow guarantees materials with a permanent porosity,[72,73] this second strategy could render alternative MOFs[74-

[77] probably showing lesser usual properties and with novel applications that might result complementary to those reported previously.

Results and Discussion

As an initial point we tackled the synthesis of Leigh-type rotaxanes **2** bearing a carboxyl group at each isophthalamide unit of its structure and with an olefin-based thread (Fig. 1a). The interlocked dicarboxylic acid (*E*)-**2** was obtained by base hydrolysis of the corresponding interlocked diester (**S1**), which was previously prepared by a five-component clipping reaction using *p*-xylylenediamine, 5-(methoxycarbonyl)isophthaloyl chloride and *N,N,N',N'*-tetrabenzylfumaramide (**1**)[78,79] as the hydrogen-bonding template (Scheme S1). The interlocked dicarboxylic acid (*Z*)-**2** was obtained in three straightforward synthetic steps from (*E*)-**2**, involving the protection of the carboxylic acid functions as 4-methoxybenzyl esters, olefin photoisomerization and acid hydrolysis of the ester groups. Both mechanically interlocked compounds **2** were fully characterized both in solution and the solid state (see Supp. Info). The molecular structure of (*E*)-**2** was also determined by X-ray crystallography (Figures 1b and S20, Tables S5 and S6), revealing the entangled relationship between the fumaramide thread and the benzylic amide macrocycle displaying the common double bifurcated H-bond pattern observed in other Leigh-type rotaxanes.[57]

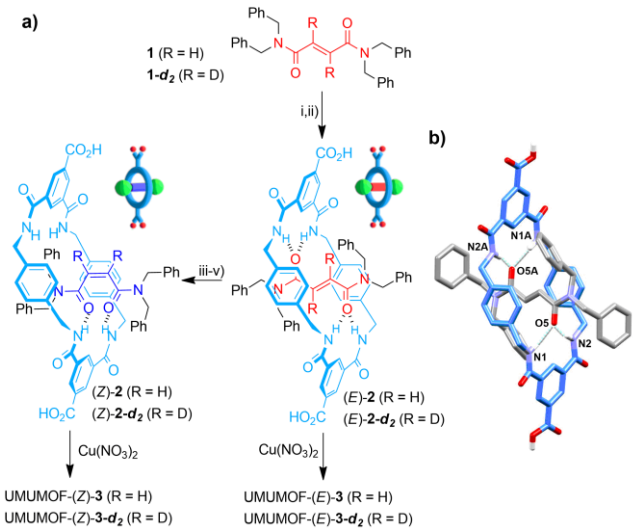

Figure 1. a) Preparation of the interlocked diacids (*E*) and (*Z*)-**2** and their corresponding metal-organic materials **3**. Reaction conditions: i) *p*-xylylenediamine, methyl 3,5-bis(chlorocarbonyl)benzoate, Et_3N, $CHCl_3$, 25 °C, 4 h (R = H, 36%; R = D, 30%); ii) LiOH, THF-H_2O, reflux, 72 h; then neutralization with HCl 6M (R = H, 79%; R = D, 72%); iii) *p*-methoxybenzyl bromide, NaI, Cs_2CO_3, DMF, 25 °C, 24 h (R = H, 91%; R = D, 95%); iv) 254 nm, CH_2Cl_2, 25 °C, 60 min (R = H, 56%; R = D, 64%); v) TFA, CH_2Cl_2, overnight (R = H, 92%; R = D, 94%). Full experimental procedures can be found in the Supporting Information. b) Stick representation of the single-crystal structure of (*E*)-**2** showing the polar hydrogen bonds involving thread donor atoms. Intramolecular hydrogen-bond lengths [Å] (and angles[º]): O5HN1/O5AHN1A 2.075 (168.2) and O5HN2/O5AHN2A 2.243 (170.0).

The hydrogen bonded rotaxane (*E*)-**2** was used as ditopic organic linker to synthesize the Cu(II)-based MOF, that we designated as UMUMOF-(*E*)-**3**, by reaction with $Cu(NO_3)_2$ in a mixture of DMF/EtOH/H_2O at 80 ºC for 48 h. Afterward, the reaction was slowly cooled to room temperature at a rate of 0.05 ºC/min (see Fig. S1), reproducibly providing a blue crystalline material in 61% yield (Fig. 1a). Elemental analysis, infrared spectroscopy, scanning electron microscopy, thermogravimetric analysis, and powder X-ray diffraction were employed for fully characterising the material after solvent exchange with chloroform and evacuation at 50 ºC under vacuum (10 torr) for 5 hours. FTIR analysis confirmed the incorporation of the copper ions into the material showing a medium-intensity band at 481 cm^{-1} corresponding to the vibrational mode of the Cu-O bond (Fig. S2b). Thermal gravimetric analysis showed a good thermal stability up to 340 ºC, whereas at that temperature a significant weight loss due to the ligand decomposition is produced (Fig. S4a). SEM micrographs of the obtained crystals regularly display a prismatic morphology with edge lengths mainly spanning in the 80-100 μm range (Image S3a). Comparison of the calculated and experimental XPRD patterns provided further evidences of the phase purity of the obtained material (Fig. S7). Also, XPRD of the desolvated material (Fig. S8) revealed that the crystallinity is retained after thermal activation under vacuum. The slight shifting and the intensity

increase of some peaks at low theta angles seems to point out the closing of the pores as one may expected from a flexible MOF.[74]

The analysis of UMUMOF-(*E*)-**3** by single-crystal X-ray diffraction (Fig. 2) showed the material to have an overall formula of $[Cu_2(\mathbf{2})_2(DMF)_2\ (H_2O)_2]$ crystallizing in the monoclinic $P2_1/n$ space group (Tables S1 and S2). The crystalline topology[80] is based on the 2-periodic *sql* net[81] of non-interpenetrated rhombohedral 4^4 grids in which the dimeric Cu(II) paddlewheel clusters of the vertices are connected through the interlocked linkers and having two water molecules coordinated at the axial positions of each dinuclear cluster. The dimensions of each rhombohedral grid is 20.7 x 20.7 $Å^2$, and the angle between two rotaxane linkers is 68.5º (Fig. 2c). These metallogrids are stacked in corrugated layers (Fig. 3 and S16) every 10.8 Å, stabilised by strong hydrogen bond interactions ($CuOH\cdots O{=}C_{macr}$: 1.931 Å) between one oxygen atom of the macrocycle of one layer and the hydrogen atom of one of the apical water molecules at the Cu(II) paddlewheel cluster of the neighbouring layer (Fig. S17). The incorporation of these interlocked units in this MOF brings a noticeable effect on the chair conformation of the macrocycle, causing the 33º dislocation of the plane of one isophthalamide moiety with respect to that containing the four methylene groups, as compared with the free ligand (*E*)-**2** (Fig. S20). Despite of this structural distortion, the interlocked components interact via the usual double bifurcated H-bond pattern (Fig. 2a). Interestingly, this particular arrangement of the layers forms channels along the a-axis partially occupied by the interlocked olefins, with an estimated solvent-accessible volume of 20% of the total volume (Fig. S18).

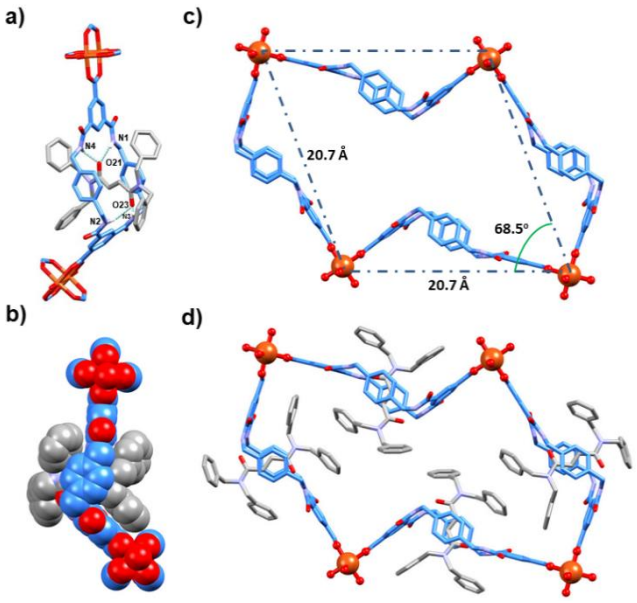

Figure 2. Structure of UMUMOF-(*E*)-**3**, $[Cu_2(\mathbf{2})_2(H_2O)_2(DMF)_2 \cdot nH_2O]$, determined by single-crystal X-ray diffraction (solvent molecules such as DMF and hydrogen atoms are omitted for clarity). (a) Stick representation of a single unit of the rotaxane linker coordinated to two Cu(II) paddlewheel clusters showing the polar hydrogen bonds between thread and ring. Intramolecular hydrogen-bond lengths [Å] (and angles[º]): O21HN1 2.458 (153.0); O21HN4 2.192 (168.9); O23HN2 2.264 (173.7) and O23HN3 2.354 (169.2). (b) CPK model of the same unit. (c) 2D Rhombohedral framework comprising four paddlewheel units having dimensions of 20.7 × 20.7 $Å^2$ (68.5º) with threads omitted. (d) The same framework showing threads.

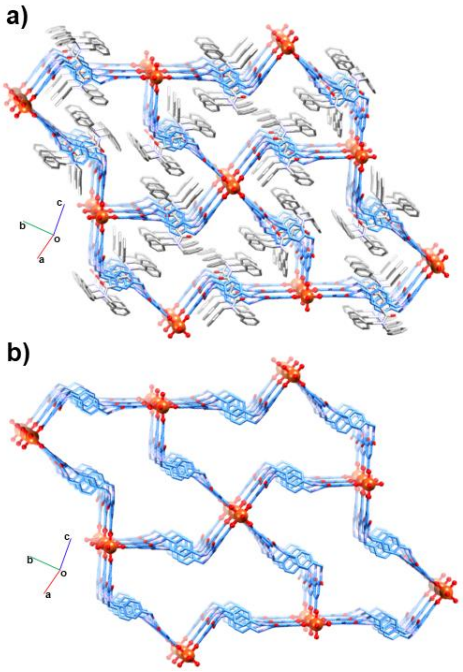

Figure 3. (a) Linked frameworks structured in a 2-periodic *sql* net showing the channels in UMUMOF-(*E*)-**3**. These 2D rhombohedral grids are stacked in a staggered manner by strong hydrogen bonds between one oxygen atom of the macrocycle of one layer and the hydrogen atom of one of the apical water molecules at the Cu(II) paddlewheel cluster of the neighboring layer (CuOH···O=C; 1.931 Å) (Fig. S17). (b) As in (a), but omitting the threads of the (*E*)-**2** coordinated rotaxane ligands for clarity.

Analogously, the rotaxane (*Z*)-**2** was used as linker to prepare the maleamide-based UMUMOF-(*Z*)-**3** by reaction with $Cu(NO_3)_2$, affording a blue crystalline material in a notably lower 22% yield (see Fig. 1a). Although we also obtained regular prismatic crystals, their X-ray reflections were too weak even using a synchrotron source, thus precluding a complete crystallographic analysis. The higher flexibility of (*Z*)-**2**, which stablishes only two polar H-bonds between the mechanically entangled components[57] instead of the four bifurcated H-bonds of (*E*)-**2**, probably precludes the acquisition of better X-ray data. Nevertheless, a partially solved structure of (*Z*)-**2** clearly showed a 2D-periodic *sql* net of non-interpenetrated rhombohedral 4^4 grids in which dimeric Cu(II) paddlewheel clusters, similar to those of (*E*)-**2**, are connected through the carboxylic acid groups of the macrocycles (Fig. S21). As in the case of

the fumaramide-based material, the phase uniformity of UMUMOF-(*Z*)-**3** was studied using the same techniques (FTIR: Fig S2c, SEM: Image S3b and XPRD: Fig S9).

At this point we rationalized that the limited room defined by the stacked rhombohedral grids might still be of enough volume to allow the configurational switch of the olefins threaded through the macrocyclic linkers. Consequently, a change of the internal dynamics of the material due to the decrease of the number H-bonds between the interlocked components would then happen.[57] Aimed to probe this hypothesis, we decided to study the dynamics[1] induced by the internal rotation of the deuterated interlocked olefin threads at the metal-organic materials by solid state ^{2}H NMR experiments. For that purpose, the corresponding UMUMOF-(*E*)-**3**-d_2 and UMUMOF-(*Z*)-**3**-d_2 were prepared from the doubly deuterated amides (*E*)-**2**-d_2 and (*Z*)-**2**-d_2 respectively by the same synthetic protocol described above (Fig. 1a). The formation of these materials was confirmed by elemental analyses and FTIR (Figs. S3a and S3b) and their stabilities were evaluated by thermogravimetric experiments (Figs. S4f and S4g) showing to be similar to those of their unlabelled surrogates.

Variable-temperature (212-373 K) solid state ^{2}H NMR experiments of both materials showed only slight variations in the broadness of the common Pake patterns[49] (Fig. S12), indicating a minimal rotation of the threads in the interlocked struts. However, during these experiments, a decrease of the signal intensities of the spectrum at 373 K in the case of UMUMOF-(*E*)-**3**-d_2, and at 333 K for UMUMOF-(*Z*)-**3**-d_2 (Fig. S12a and S12b) was noted indicating the onset of intermediate rotational regime motions.[82,83] These observations qualitatively allow to attribute a lower rotational energy barrier[84-86] to UMUMOF-(*Z*)-**3**-d_2 compared to that of UMUMOF-(*E*)-**3**-d_2. We reasoned that the larger barrier of UMUMOF-(*E*)-**3**-d_2 is due to the slower motion of the fumaramide rods, which establish four N-H···O=C hydrogen bonds with their respective macrocyclic linkers in comparison with the maleamide rods of UMUMOF-(*Z*)-**3**-d_2, which only form two (Fig. 4). As we expected, the relationship between the rotational energy barriers of the rods in these materials is in full agreement with that described for the pirouetting motions in simple tetrasubstituted fumaramide and maleamide rotaxanes.[57] We remark that the internal dynamics

of these materials is much slower than that observed in materials having crown-ether based rotaxanes as linkers described by Loeb,[46] in which the intercomponent interaction strength is smaller than that of the amide-based ones shown here.

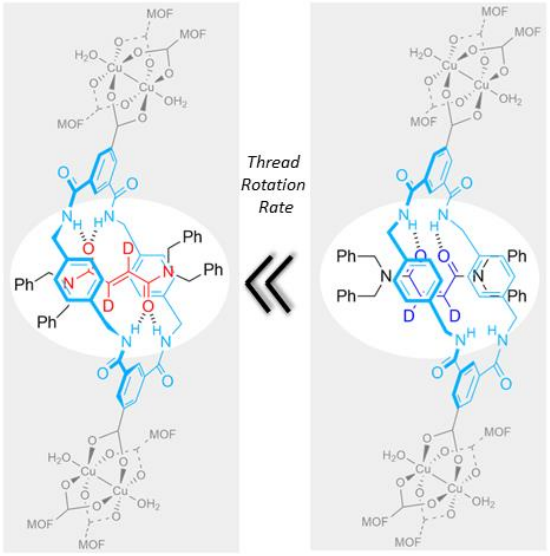

Figure 4. Relationship between the rotational motions of the deuterium labelled metal-organic materials UMUMOF-(*E*)-**3**-d_2 and UMUMOF-(*Z*)-**3**-d_2 resulting from variable-temperature solid state ^{2}H NMR experiments.

The synthesized metal-organic materials could be structurally modified, with a change of the thread geometry of the interlocked struts, by applying a light stimulus (Fig. 5). We established that the photoisomerization of a suspension of pristine UMUMOF-(*E*)-**3** in dichloromethane using a 312 nm light source led to a material composed by 80% of (*E*)-**2** and 20% of (*Z*)-**2** as confirmed by an acid digestion of the irradiated material UMUMOF-($E_{80}Z_{20}$)-**3** (Fig. 5a and Image S2). On the other hand, the irradiation of pristine UMUMOF-(*Z*)-**3** under the same conditions afforded the complementary metal-organic framework UMUMOF-($E_{20}Z_{80}$)-**3**, having the inverse isomeric ratio of threads than the previous one, 20% of fumaramide and 80% of maleamide (Fig. 5b). In contrast with the isomerization experiments in solution, a common photoestationary state was unreachable at the solid state, probably, due to a different interaction mode of the light[53] with both metal organic materials. Aimed to gain further knowledge on this phenomenon, we studied the photoisomerization process by means different

wavelengths and irradiation periods using materials of varied crystal sizes (Tables S1 and S2). The use of 254 nm light or extended irradiation times (24 h) did not afford higher isomerization ratios, causing a notable level of decomposition of the organic linkers. When finely milled materials were irradiated (312 nm, 8 h), no effect of the crystal size was observed in the isomerization process of UMUMOF-(*E*)-**3**. In contrast, the microcrystalline UMUMOF-(*Z*)-**3** underwent a higher level of *Z* to *E* isomerization (to 40:60, *E*:*Z*) under the same irradiation conditions. We also proved that the thermal treatment at 140 ºC of all the maleamide-containing materials returns the *trans* configuration to all interlocked olefins.

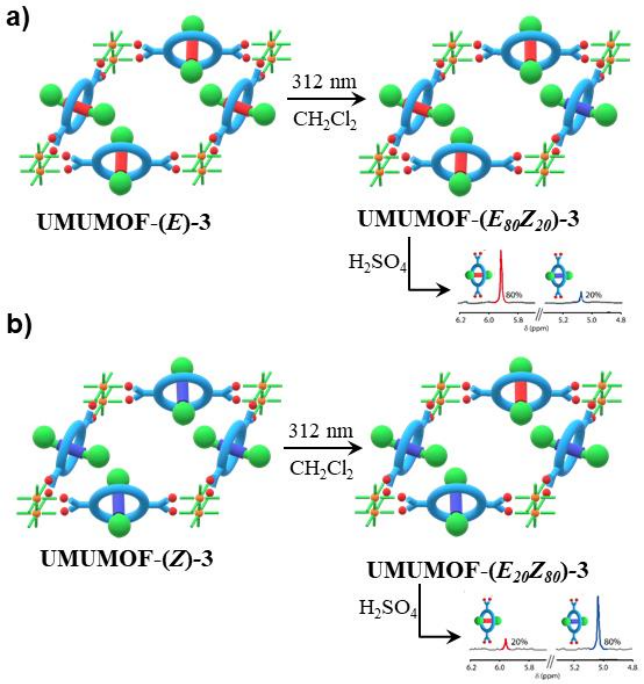

Figure 5. Irradiation processes at 312 nm of pristine (a) UMUMOF-(*E*)-**3** and (b) UMUMOF-(*Z*)-**3** and the selected fragments of ^{1}H NMR spectra (DMSO-d_6, 400 MHz, 298 K; range: 4.8-5.3 and 5.7-6.2 ppm) resulting from the acid digestion of the *E*/*Z*-mixed materials showing the ratio of (*E*)-**2** and (*Z*)-**2** linkers. Cartoons of UMUMOF-($E_{80}Z_{20}$)-**3** and UMUMOF-($E_{20}Z_{80}$)-**3** only disclose an illustrative ratio of the *E*/*Z* rotaxanes linkers.

An important consequence of the *E*/*Z* configurational changes at the interlocked olefins lies on the variation of the available free volume into the channels of the respective UMUMOFs. In order to explore this structural alteration and the potential use of these materials as molecular dispensers, we decided to

carry out a study of load and photorelease of *p*-benzoquinone (Q) as a model cargo (Fig. 6a). The light blue coloured UMUMOF-(*E*)-**3** was loaded with *p*-benzoquinone by suspending the material in a 1.2 M solution of the cargo in chloroform for 8 h. After filtering and exhaustively washing, a greenish blue material Q@UMUMOF-(*E*)-**3** (Image S1) was isolated, which contained a 9.82% w/w of the quinone (see Supporting Information for further details). The release of this cargo from the loaded MOF material was explored under different conditions, varying the solvent and temperature. This exploration revealed that the presence of highly competitive H-bonding solvents promotes a quicker liberation of the quinone. In DMF the cargo is fully liberated in less than 1 h, the same operation requires 8 h in MeOH and the discharge takes more than 1.5 days in THF (Fig. S5). Interestingly, *p*-benzoquinone is reasonably retained inside the MOF when the loaded material is suspended in dichloromethane at 25 ºC only observing a minimal leaking (less than 5%) (Fig. 6b, blue line). As we expected, this cargo release can be speeded up by warming the solution to 40 ºC to get out 20% of the quinone (Fig. 6b, red line). Interestingly, by irradiating Q@UMUMOF-(*E*)-**3** at 312 nm, we were able to promote a controlled release of the cargo during 8 hours at 25 ºC (Fig. 6b, green line) as consequence of the isomerization of the interlocked linkers. Note that the quinone loaded Q@UMUMOF-(*Z*)-**3** (12.34% w/w) is fully discharged in only 2 hours at room temperature in darkness when suspended in dichloromethane (Fig. 6b, purple line). To explain this result, we hypothesized that the photoisomerization could promote some kind of MOF breathing[87-89] that triggers the cargo release as result of the variation of the pore size of the metal organic material. In fact, we analysed the porosity of these materials by nitrogen adsorption experiments founding that the porosity grows as the percentage of maleamide threads in the interlocked linkers increases (see Table S7).

Finally, the efficiency of one of these materials as dispenser was evaluated by an iterability study by doing repeated cycles in which UMUMOF-(*E*)-**3** was loaded with *p*-benzoquinone, discharged by irradiation at 312 nm and thermally re-isomerized, before starting the next cycle (Figs. S10 and S11).

This evaluation showed a good reusability, the material retaining a cargo capacity close to 80% after three cycles (Fig 6c).

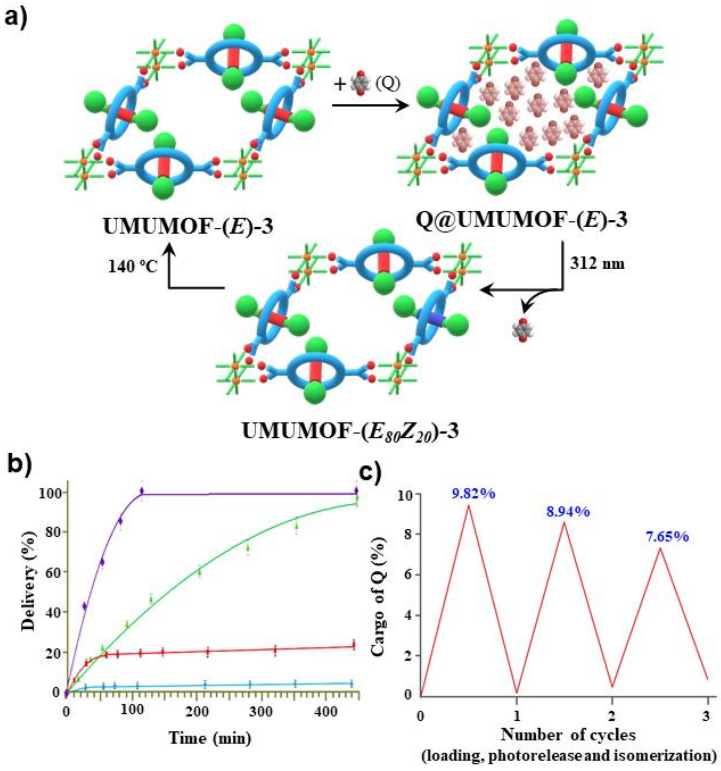

Figure 6. (a) Cyclic working of the UMUMOF-(*E*)-**3** as metal organic dispenser of *p*-benzoquinone (Q). This operation consists of three steps: cargo loading (filtering, washing and drying), photorelease and thermal recovery. (b) Cargo release plots from Q@UMUMOF-(*E*)-**3** in DCM at 25 ºC (blue line), at 40 ºC (red line) and irradiating at a wavelength of 312 nm (green line), for a period of 8 hours in all cases. For comparison, the release plot of *p*-benzoquinone from Q@UMUMOF-(*Z*)-**3** in DCM at 25 ºC (purple line) has been also included. In these studies, the amount of the released quinone was monitored by gas chromatography using 1,4-dibromobenzene as internal standard. (c) Iterability analysis showing three working cycles and the corresponding quinone loading capacity after each cycle supported by XPRD measurements after each step (Fig. S11). Cartoon of UMUMOF-($E_{80}Z_{20}$)-**3** only discloses an illustrative ratio of the *E/Z* rotaxanes linkers.

Conclusions

In summary, we have prepared a photoresponsive metal organic material in a reproducible manner using a benzylic amide [2]rotaxane as linker and copper(II) ions as metal nodes. Single crystal X-ray diffraction analysis unveiled the formation of a robust structure consisting of stacked 2D rhombohedral grids which form channels integrating interlocked alkenyl threads. By dynamic solid state ^{2}H NMR measurements using deuterium-labelled materials we proved that changes in the geometry of the olefinic axis of the interlocked struts induced different independent local dynamics as a direct consequence of the variation in the strength of the intercomponent non-covalent interactions. A photoisomerization process of the interlocked unsaturated threads granted the access to two rotaxane-based materials having linkers with variable *E/Z* olefin ratios. One of these materials, UMUMOF-(*E*)-**3**. has been profitably employed as a photocontrollable nanodispenser of *p*-benzoquinone as a model molecular cargo. The novel alternative approach shown here for arraying molecular machine constituents into MOFs should be added to the current toolbox of protocols for building novel functional rotaxane-based materials.

Acknowledgements. This work was supported by the MINECO (CTQ2014-56887-P and CTQ2017-87231-P) with joint financing by FEDER Funds and Fundación Seneca-CARM (Project 20811/PI/18). A.M.-C. thanks MICINN for a Ramon y Cajal contract and funding (RYC-2017-22700). A. S.-S. also thanks the Fundación Seneca-CARM for his PhD fellowship. M.R.B. and M.A.P.M. are grateful to the CAPES and CNPq agencies. We gratefully acknowledge Dr. Elisa Barea for insightful discussions. The NMR facility of the ICMM-CSIC and ACTI-UM are acknowledged for its assistance.

Supporting Information Available: Experimental procedures, characterization data for all new compounds and materials, and full crystallographic details of rotaxane (*E*)-**2** and UMUMOF-(*E*)-**3** including cif files. This material is available free of charge via the Internet at http://pubs.acs.org.

Competing interests

The authors declare no competing interests.

References

(1) Yaghi, O. M.; Kalmutzki, M. J.; Diercks, C. S. *Introduction to Reticular Chemistry: Metal-Organic Frameworks and Covalent Organic Frameworks*, 1st ed.; Wiley, 2019. https://doi.org/10.1002/9783527821099.

(2) García, H.; Navalón, S. *Metal-Organic Frameworks: Applications in Separations and Catalysis*; García, H., Navalón, S., Eds.; Wiley-VCH Verlag GmbH & Co. KGaA: Weinheim, Germany, 2018. https://doi.org/10.1002/9783527809097.

(3) Li, H.; Eddaoudi, M.; O'Keeffe, M.; Yaghi, O. M. Design and Synthesis of an Exceptionally Stable and Highly Porous Metal-Organic Framework. *Nature* **1999**, *402* (6759), 276–279. https://doi.org/10.1038/46248.

(4) James, S. L. Metal-Organic Frameworks. *Chem. Soc. Rev.* **2003**, *32* (5), 276–288. https://doi.org/10.1039/b200393g.

(5) Li, Q.; Zhang, W.; Miljanic, O. S.; Sue, C.-H.; Zhao, Y.-L.; Liu, L.; Knobler, C. B.; Stoddart, J. F.; Yaghi, O. M. Docking in Metal-Organic Frameworks. *Science* **2009**, *325* (5942), 855–859. https://doi.org/10.1126/science.1175441.

(6) Smaldone, R. A.; Forgan, R. S.; Furukawa, H.; Gassensmith, J. J.; Slawin, A. M. Z.; Yaghi, O. M.; Stoddart, J. F. Metal-Organic Frameworks from Edible Natural Products. *Angew. Chem., Int. Ed.* **2010**, *49* (46), 8630–8634, S8630/1-S8630/13. https://doi.org/10.1002/anie.201002343.

(7) Furukawa, H.; Cordova, K. E.; O'Keeffe, M.; Yaghi, O. M. The Chemistry and Applications of Metal-Organic Frameworks. *Science* **2013**, *341* (6149), 1230444–1230444. https://doi.org/10.1126/science.1230444.

(8) Van Vleet, M. J.; Weng, T.; Li, X.; Schmidt, J. R. In Situ, Time-Resolved, and Mechanistic Studies of Metal–Organic Framework Nucleation and Growth. *Chem. Rev.* **2018**, *118* (7), 3681–3721. https://doi.org/10.1021/acs.chemrev.7b00582.

(9) Yuan, S.; Feng, L.; Wang, K.; Pang, J.; Bosch, M.; Lollar, C.; Sun, Y.; Qin, J.; Yang, X.; Zhang, P.; Wang, Q.; Zou, L.; Zhang, Y.; Zhang, L.; Fang, Y.; Li, J.; Zhou, H.-C. Stable Metal–Organic

Frameworks: Design, Synthesis, and Applications. *Adv. Mater.* **2018**, *30* (37), 1704303. https://doi.org/10.1002/adma.201704303.

(10) Vogelsberg, C. S.; Garcia-Garibay, M. A. Crystalline Molecular Machines: Function, Phase Order, Dimensionality, and Composition. *Chem. Soc. Rev.* **2012**, *41* (5), 1892–1910. https://doi.org/10.1039/c1cs15197e.

(11) Moulin, E.; Faour, L.; Carmona-Vargas, C. C.; Giuseppone, N. From Molecular Machines to Stimuli-Responsive Materials. *Adv. Mater.* **2019**, 1906036. https://doi.org/10.1002/adma.201906036.

(12) Danowski, W.; van Leeuwen, T.; Abdolahzadeh, S.; Roke, D.; Browne, W. R.; Wezenberg, S. J.; Feringa, B. L. Unidirectional Rotary Motion in a Metal–Organic Framework. *Nat. Nanotechnol.* **2019**, *14* (5), 488–494. https://doi.org/10.1038/s41565-019-0401-6.

(13) Mena-Hernando, S.; Pérez, E. M. Mechanically Interlocked Materials. Rotaxanes and Catenanes beyond the Small Molecule. *Chem. Soc. Rev.* **2019**, *48* (19), 5016–5032. https://doi.org/10.1039/C8CS00888D.

(14) Abendroth, J. M.; Bushuyeb, O. S.; Weiss, P. S.;Barret, C. J. Controlling Motion at the Nanoscale: Rise of the Molecular Machines. *ACS Nano* **2015**, *9* (8), 7746-7768. https://doi.org/10.1021/acsnano.5b03367.

(15) Xue, M.; Yang, Y.; Chi, X.; Yan, X.; Huang, F. Development of Pseudorotaxanes and Rotaxanes: From Synthesis to Stimuli-Responsive Motions to Applications. *Chem. Rev.* **2015**, *115* (15), 7398–7501. https://doi.org/10.1021/cr5005869.

(16) Erbas-Cakmak, S.; Leigh, D. A.; McTernan, C. T.; Nussbaumer, A. L. Artificial Molecular Machines. *Chem. Rev.* **2015**, 115, 10081-10206. https://doi.org/10.1021/acs.chemrev.5b00146.

(17) Leigh, D. A. Genesis of the Nanomachines: The 2016 Nobel Prize in Chemistry. *Angew. Chem., Int. Ed.* **2016**, *55* (47), 14506–14508. https://doi.org/10.1002/anie.201609841.

(18) Lewis, J. E. M.; Beer, P. D.; Loeb, S. J.; Goldup, S. M. Metal Ions in the Synthesis of Interlocked Molecules and Materials. *Chem. Soc. Rev.* **2017**, *46* (9), 2577–2591. https://doi.org/10.1039/C7CS00199A.

(19) Pezzato, C.; Cheng, C.; Stoddart, J. F.; Astumian, R. D. Mastering the Non-Equilibrium Assembly and Operation of Molecular Machines. *Chem. Soc. Rev.* **2017**, *46* (18), 5491–5507. https://doi.org/10.1039/C7CS00068E.

(20) Kassem, S.; van Leeuwen, T.; Lubbe, A. S.; Wilson, M. R.; Feringa, B. L.; Leigh, D. A. Artificial Molecular Motors. *Chem. Soc. Rev.* **2017**, *46* (9), 2592–2621. https://doi.org/10.1039/C7CS00245A.

(21) Feringa, B. L. The Art of Building Small: From Molecular Switches to Motors (Nobel Lecture). *Angew. Chem., Int. Ed.* **2017**, *56* (37), 11060–11078. https://doi.org/10.1002/anie.201702979.

(22) Stoddart, J. F. Mechanically Interlocked Molecules (MIMs)-Molecular Shuttles, Switches, and Machines (Nobel Lecture). *Angew. Chem., Int. Ed.* **2017**, *56* (37), 11094–11125. https://doi.org/10.1002/anie.201703216.

(23) Sauvage, J.-P. From Chemical Topology to Molecular Machines (Nobel Lecture). *Angew. Chem., Int. Ed.* **2017**, *56* (37), 11080–11093. https://doi.org/10.1002/anie.201702992.

(24) Inthasot, A.; Tung, S.-T.; Chiu, S.-H. Using Alkali Metal Ions To Template the Synthesis of Interlocked Molecules. *Acc. Chem. Res.* **2018**, *51* (6), 1324–1337. https://doi.org/10.1021/acs.accounts.8b00071.

(25) Jamieson, E. M. G.; Modicom, F.; Goldup, S. M. Chirality in Rotaxanes and Catenanes. *Chem. Soc. Rev.* **2018**, *47* (14), 5266–5311. https://doi.org/10.1039/C8CS00097B.

(26) Yang, K.; Chao, S.; Zhang, F.; Pei, Y.; Pei, Z. Recent Advances in the Development of Rotaxanes and Pseudorotaxanes Based on Pillar[n]Arenes: From Construction to Application. *Chem. Commun.* **2019**, *55* (88), 13198–13210. https://doi.org/10.1039/c9cc07373f.

(27) Baroncini, M.; Silvi, S.; Credi, A. Photo- and Redox-Driven Artificial Molecular Motors. *Chem. Rev.* **2020**, *120* (1), 200–268. https://doi.org/10.1021/acs.chemrev.9b00291.

(28) Aprahamian, I. The Future of Molecular Machines. *ACS Cent. Sci.* **2020**, *6* (3), 347–358. https://doi.org/10.1021/acscentsci.0c00064.

(29) Sluysmans, D.; Stoddart, J. F. The Burgeoning of Mechanically Interlocked Molecules in Chemistry. *Trends in Chemistry* **2019**, *1 (2)*, 185-197. https://doi.org/10.1016/j.trechm.2019.02.013.

(30) Ambrogio, M. W.; Thomas, C. R.; Zhao, Y.-L.; Zink, J. I.; Stoddart, J. F. Mechanized Silica Nanoparticles: A New Frontier in Theranostic Nanomedicine. *Acc. Chem. Res.* **2011**, *44* (10), 903–913. https://doi.org/10.1021/ar200018x.

(31) Yang, Y. W.; Sun, Y. L.; Song, N. Switchable Host-Guest Systems on Surfaces. *Acc. Chem. Res.* **2014**, *47* (7), 1950–1960. https://doi.org/10.1021/ar500022f.

(32) Harada, A.; Takashima, Y.; Nakahata, M. Supramolecular Polymeric Materials via Cyclodextrin-Guest Interactions. *Acc. Chem. Res.* **2014**, *47* (7), 2128–2140. https://doi.org/10.1021/ar500109h.

(33) Wang, Y.; Ping, G.; Li, C. Efficient Complexation between Pillar[5]Arenes and Neutral Guests: From Host–Guest Chemistry to Functional Materials. *Chem. Commun.* **2016**, *52* (64), 9858–9872. https://doi.org/10.1039/C6CC03999E.

(34) Li, Q.; Zhang, W.; Miljanic, O. S.; Knobler, C. B.; Stoddart, J. F.; Yaghi, O. M. A metal-organic framework replete with ordered donor-acceptor catenanes. *Chem. Commun*. **2010**, 46, 380-382. https://doi.org/10.1039/B919923C.

(35) Zhao, Y.-L.; Liu, L.; Zhang, W.; Sue, C.-H.; Li, Q.; Miljanic, O. S.; Yaghi, O. M.; Stoddart, J. F. Rigid-Strut-Containing Crown Ethers and [2]Catenanes for Incorporation into Metal-Organic Frameworks. *Chem. Eur. J*. **2009**, 14, 13356-13380. https://doi.org/10.1002/chem.200902350.

(36) Martinez-Bulit, P.; Stirk, A. J.; Loeb, S. J. Rotors, Motors, and Machines Inside Metal-Organic Frameworks. *Trends in Chemistry* **2019**, 1, 588-600. https://doi.org/10.1016/j.trechm.2019.05.005.

(37) Loeb, S. J. Metal–Organic Rotaxane Frameworks; MORFs. *Chem. Commun.* **2005**, No. 12, 1511–1518. https://doi.org/10.1039/B416609D.

(38) Loeb, S. J. Rotaxanes as Ligands: From Molecules to Materials. *Chem. Soc. Rev.* **2007**, *36* (2), 226–235. https://doi.org/10.1039/B605172N.

(39) Zhu, K.; Loeb, S. J. Organizing Mechanically Interlocked Molecules to Function inside Metal-Organic Frameworks. *Top. Curr. Chem.* **2014**, *354*, 213–251. https://doi.org/10.1007/128_2013_516.

(40) Yang, Y.-D.; Fan, C.-C.; Rambo, B. M.; Gong, H.-Y.; Xu, L.-J.; Xiang, J.-F.; Sessler, J. L. Multicomponent Self-Assembled Metal-Organic [3]Rotaxanes. *J. Am. Chem. Soc.* **2015**, *137 (40)*, 12966-12976. https://doi.org/10.1021/jacs.5b07308.

(41) Chen, X.-L.; Shen, Y.-J.; Gao, C.; Yang, J.; Sun, X.; Zhang, X.; Yang, Y.-D.; Wei, G.-P.; Xiang, J.-F., Sessler, J. L.; Gong, H.-Y. Regulating the Structures of Self-Assembled Mechanically Interlocked Molecular Constructs via Dianion Substituent Effects. *J. Am. Chem. Soc.* **2020**, *142* (16), 7443-7455. https://dx.doi.org/10.1021/jacs.9b13473.

(42) Whang, D.; Kim, K. Polycatenated Two-Dimensional Polyrotaxane Net. *J. Am. Chem. Soc.* **1997**, *119* (2), 451–452. https://doi.org/10.1021/JA963096Z.

(43) Lee, E.; Heo, J.; Kim, K. A Three-Dimensional Polyrotaxane Network. *Angew. Chem., Int. Ed.* **2000**, *39* (15), 2699–2701. https://doi.org/10.1002/1521-3773(20000804)39:15<2699::AID-ANIE2699>3.0.CO;2-Z.

(44) Lee, E.; Kim, J.; Heo, J.; Whang, D.; Kim, K. A Two-Dimensional Polyrotaxane with Large Cavities and Channels: A Novel Approach to Metal-Organic Open-Frameworks by Using Supramolecular Building Blocks. *Angew. Chem., Int. Ed.* **2001**, *40* (2), 399–402. https://doi.org/10.1002/1521-3773(20010119)40:2<399::AID-ANIE399>3.0.CO;2-W.

(45) Vukotic, V. N.; Harris, K. J.; Zhu, K.; Schurko, R. W.; Loeb, S. J. Metal–Organic Frameworks with Dynamic Interlocked Components. *Nat. Chem.* **2012**, *4*, 456. https://doi.org/10.1038/nchem.1354.

(46) Vukotic, V. N.; O'Keefe, C. A.; Zhu, K.; Harris, K. J.; To, C.; Schurko, R. W.; Loeb, S. J. Mechanically Interlocked Linkers inside Metal–Organic Frameworks: Effect of Ring Size on Rotational Dynamics. *J. Am. Chem. Soc.* **2015**, *137* (30), 9643–9651. https://doi.org/10.1021/jacs.5b04674.

(47) Zhu, K.; O'Keefe, C. A.; Vukotic, V. N.; Schurko, R. W.; Loeb, S. J. A Molecular Shuttle That Operates inside a Metal–Organic Framework. *Nat. Chem.* **2015**, *7* (6), 514–519. https://doi.org/10.1038/nchem.2258.

(48) Gholami, G.; Wilson, B. H.; Zhu, K.; O'Keefe, C. A.; Schurko, R. W.; Loeb, S. J. Exploring the Dynamics of Zr-Based Metal-organic Frameworks Containing Mechanically Interlocked Molecular Shuttles. *Faraday Discuss.* **2020**, 10.1039.D0FD00004C. https://doi.org/10.1039/D0FD00004C.

(49) Hansen, M. R.; Graf, R.; Spiess, H. W. Solid-State NMR in Macromolecular Systems: Insights on How Molecular Entities Move. *Acc. Chem. Res.* **2013**, *46* (9), 1996–2007. https://doi.org/10.1021/ar300338b.

(50) Zhu, K.; Vukotic, V. N.; O'Keefe, C. A.; Schurko, R. W.; Loeb, S. J. Metal–Organic Frameworks with Mechanically Interlocked Pillars: Controlling Ring Dynamics in the Solid-State via a Reversible Phase Change. *J. Am. Chem. Soc.* **2014**, *136* (20), 7403–7409. https://doi.org/10.1021/ja502238a.

(51) Coskun, A.; Hmadeh, M.; Barin, G.; Gándara, F.; Li, Q.; Choi, E.; Strutt, N. L.; Cordes, D. B.; Slawin, A. M. Z.; Stoddart, J. F.; Sauvage, J.-P.; Yaghi, O. M. Metal-Organic Frameworks Incorporating Copper-Complexed Rotaxanes. *Angew. Chem., Int. Ed.* **2012**, *51* (9), 2160–2163. https://doi.org/10.1002/anie.201107873.

(52) McGonigal, P. R.; Deria, P.; Hod, I.; Moghadam, P. Z.; Avestro, A.-J.; Horwitz, N. E.; Gibbs-Hall, I. C.; Blackburn, A. K.; Chen, D.; Botros, Y. Y.; Wasielewski, M. R.; Snurr, R. Q.; Hupp, J. T.; Farha, O. K.; Stoddart, J. F. Electrochemically Addressable Trisradical Rotaxanes Organized within a Metal-Organic Framework. *Proc. Natl. Acad. Sci. USA* **2015**, *112* (36), 11161–11168. https://doi.org/10.1073/pnas.1514485112.

(53) Haldar, R.; Heinke, L.; Woell, C. Advanced Photoresponsive Materials Using the Metal-Organic Framework Approach. *Adv. Mater.* **2019**, 1905227. https://doi.org/10.1002/adma.201905227.

(54) Gatti, F. G.; Leigh, D. A; Nepogodiev, S. A; Slawin, A. M. Z.; Teat, S. J.; Wong, J. K. Y. Stiff, and Sticky in the Right Places: The Dramatic Influence of Preorganizing Guest Binding Sites on the Hydrogen Bond-Directed Assembly of Rotaxanes. *J. Am. Chem. Soc.* **2001**, *123* (25), 5983–5989. https://doi.org/10.1021/ja001697r.

(55) Brouwer, A. M.; Frochot, C.; Gatti, F. G.; Leigh, D. A.; Mottier, L.; Paolucci, F.; Roffia, S.; Wurpel, G. W. H. Reversible Translational Motion in a Hydrogen-Bonded Molecular Shuttle. *Science.* **2001**, *291* (5511), 2124–2128. https://doi.org/10.1126/science.1057886.

(56) Berna, J.; Leigh, D. A.; Lubomska, M.; Mendoza, S. M.; Perez, E. M.; Rudolf, P.; Teobaldi, G.; Zerbetto, F. Macroscopic Transport by Synthetic Molecular Machines. *Nat. Mater.* **2005**, *4* (9), 704–710. https://doi.org/10.1038/nmat1455.

(57) Gatti, F. G.; Leon, S.; Wong, J. K. Y.; Bottari, G.; Altieri, A.; Morales, M. A. F.; Teat, S. J.; Frochot, C.; Leigh, D. A.; Brouwer, A. M.; Zerbetto, F. Photoisomerization of a Rotaxane Hydrogen Bonding Template: Light-Induced Acceleration of a Large Amplitude Rotational Motion. *Proc. Natl. Acad. Sci. USA* **2003**, *100* (1), 10–14. https://doi.org/10.1073/pnas.0134757100.

(58) Altieri, A.; Bottari, G.; Dehez, F.; Leigh, D. A.; Wong, J. K. Y.; Zerbetto, F. Remarkable Positional Discrimination in Bistable Light- and Heat-Switchable Hydrogen-Bonded Molecular Shuttles. *Angew. Chem., Int. Ed.* **2003**, *42* (20), 2296–2300. https://doi.org/10.1002/anie.200250745.

(59) Martinez-Cuezva, A.; Valero-Moya, S.; Alajarin, M.; Berna, J. Light-Responsive Peptide [2]Rotaxanes as Gatekeepers of Mechanised Nanocontainers. *Chem. Commun.* **2015**, *51* (77), 14501–14504. https://doi.org/10.1039/C5CC04365D.

(60) Martinez-Cuezva, A.; Saura-Sanmartin, A.; Nicolas-Garcia, T.; Navarro, C.; Orenes, R.-A.; Alajarin, M.; Berna, J. Photoswitchable Interlocked Thiodiglycolamide as a Cocatalyst of a Chalcogeno-Baylis–Hillman Reaction. *Chem. Sci.* **2017**, *8* (5), 3775–3780. https://doi.org/10.1039/C7SC00724H.

(61) Liu, W.; Gomez-Duran, C. F. A.; Smith, B. D. Fluorescent Neuraminidase Assay Based on Supramolecular Dye Capture After Enzymatic Cleavage. *J. Am. Chem. Soc.* **2017**, *139* (18), 6390–6395. https://doi.org/10.1021/jacs.7b01628.

(62) Leigh, D. A.; Marcos, V.; Nalbantoglu, T.; Vitorica-Yrezabal, I. J.; Yasar, F. T.; Zhu, X. Pyridyl-Acyl Hydrazone Rotaxanes and Molecular Shuttles. *J. Am. Chem. Soc.* **2017**, *139* (20), 7104–7109. https://doi.org/10.1021/jacs.7b03307.

(63) Saura-Sanmartin, A.; Martinez-Cuezva, A.; Pastor, A.; Bautista, D.; Berna, J. Light-Driven Exchange between Extended and Contracted Lasso-like Isomers of a Bistable [1]Rotaxane. *Org. Biomol. Chem.* **2018**, *16* (38), 6980–6987. https://doi.org/10.1039/C8OB02234H.

(64) Kumpulainen, T.; Panman, M. R.; Bakker, B. H.; Hilbers, M.; Woutersen, S.; Brouwer, A. M. Accelerating the Shuttling in Hydrogen-Bonded Rotaxanes: Active Role of the Axle and the End Station. *J. Am. Chem. Soc.* **2019**, *141* (48), 19118–19129. https://doi.org/10.1021/jacs.9b10005.

(65) Evans, N. H. Recent Advances in the Synthesis and Application of Hydrogen Bond Templated Rotaxanes and Catenanes. *Eur. J. Org. Chem.* **2019**, *2019* (21), 3320–3343. https://doi.org/10.1002/ejoc.201900081.

(66) Lopez-Maya, E.; Montoro, C.; Rodriguez-Albelo, L. M.; Aznar Cervantes, S. D.; Lozano-Perez, A. A.; Cenis, J. L.; Barea, E.; Navarro, J. A. R. Textile/Metal-Organic-Framework Composites as Self-Detoxifying Filters for Chemical-Warfare Agents. *Angew. Chem., Int. Ed.* **2015**, *54* (23), 6790–6794. https://doi.org/10.1002/anie.201502094.

(67) Zheng, H.; Zhang, Y.; Liu, L.; Wan, W.; Guo, P.; Nyström, A. M.; Zou, X. One-Pot Synthesis of Metal–Organic Frameworks with Encapsulated Target Molecules and Their Applications for Controlled Drug Delivery. *J. Am. Chem. Soc.* **2016**, *138* (3), 962–968. https://doi.org/10.1021/jacs.5b11720.

(68) Gil-San-Millan, R.; Lopez-Maya, E.; Hall, M.; Padial, N. M.; Peterson, G. W.; DeCoste, J. B.; Rodriguez-Albelo, L. M.; Oltra, J. E.; Barea, E.; Navarro, J. A. R. Chemical Warfare Agents Detoxification Properties of Zirconium Metal-Organic Frameworks by Synergistic Incorporation of Nucleophilic and Basic Sites. *ACS Appl. Mater. Interfaces* **2017**, *9* (28), 23967–23973. https://doi.org/10.1021/acsami.7b06341.

(69) Chen, X.; Tong, R.; Shi, Z.; Yang, B.; Liu, H.; Ding, S.; Wang, X.; Lei, Q.; Wu, J.; Fang, W. MOF Nanoparticles with Encapsulated Autophagy Inhibitor in Controlled Drug Delivery System for Antitumor. *ACS Appl. Mater. Interfaces* **2018**, *10* (3), 2328–2337. https://doi.org/10.1021/acsami.7b16522.

(70) Rojas, S.; Colinet, I.; Cunha, D.; Hidalgo, T.; Salles, F.; Serre, C.; Guillou, N.; Horcajada, P. Toward Understanding Drug Incorporation and Delivery from Biocompatible Metal–Organic Frameworks in View of Cutaneous Administration. *ACS Omega* **2018**, *3* (3), 2994–3003. https://doi.org/10.1021/acsomega.8b00185.

(71) Mercer, D. J.; Vukotic, V. N.; Loeb, S. J. Linking [2]Rotaxane Wheels to Create a New Type of Metal Organic Rotaxane Framework. *Chem. Commun.* **2011**, *47* (3), 896–898. https://doi.org/10.1039/C0CC04139D.

(72) Deng, H.; Olson, M. A.; Stoddart, J. F.; Yaghi, O. M. Robust dynamics. *Nat. Chem*. **2010**, 2, 439-443. https://doi.org/10.1038/nchem.654.

(73) Zhu, K.; Loeb, S. J. Organizing Mechanically Interlocked Molecules to Function Inside Metal-Organic Frameworks. In *Molecular Machines and Motors*; Credi, A., Silvi, S., Venturi, M., Eds.; Springer International Publishing: Cham, 2014; Vol. 354, pp 213–251. https://doi.org/10.1007/128_2013_516.

(74) Martí-Gastaldo, C.; Antypov, D.; Warren, J. E.; Briggs, M. E.; Chater, P. A.; Wiper, P. V.; Miller, G. J.; Khimyak, Y. Z.; Darling, G. R.; Berry, N. G.; Rosseinsky, M. J. Side-Chain Control of Porosity Closure in Single-and Multiple-Peptide-Based Porous Materials by Cooperative Folding. *Nat. Chem.* **2014**, *6* (4), 343–351. https://doi.org/10.1038/nchem.1871.

(75) Schneemann, A.; Bon, V.; Schwedler, I.; Senkovska, I.; Kaskel, S.; Fischer, R. A. Flexible Metal–Organic Frameworks. *Chem. Soc. Rev.* **2014**, *43* (16), 6062–6096. https://doi.org/10.1039/C4CS00101J.

(76) Navarro-Sanchez, J.; Argente-García, A. I.; Moliner-Martínez, Y.; Roca-Sanjuan, D.; Antypov, D.; Campíns-Falco, P.; Rosseinsky, M. J.; Marti-Gastaldo, C. Peptide Metal–Organic Frameworks for Enantioselective Separation of Chiral Drugs. *J. Am. Chem. Soc.* **2017**, *139* (12), 4294–4297. https://doi.org/10.1021/jacs.7b00280.

(77) Zhang, J.-P.; Zhou, H.-L.; Zhou, D.-D.; Liao, P.-Q.; Chen, X.-M. Controlling Flexibility of Metal–Organic Frameworks. *Natl. Sci. Rev.* **2018**, *5* (6), 907–919. https://doi.org/10.1093/nsr/nwx127.

(78) Martinez-Cuezva, A.; Lopez-Leonardo, C.; Bautista, D.; Alajarin, M.; Berna, J. Stereocontrolled Synthesis of β-Lactams within [2]Rotaxanes: Showcasing the Chemical Consequences of the Mechanical Bond. *J. Am. Chem. Soc.* **2016**, *138* (28), 8726–8729. https://doi.org/10.1021/jacs.6b05581.

(79) Lopez-Leonardo, C.; Martinez-Cuezva, A.; Bautista, D.; Alajarin, M.; Berna, J. Homo and Heteroassembly of Amide-Based [2]Rotaxanes Using α, α ′-Dimethyl- *p* -Xylylenediamines. *Chem. Commun.* **2019**, *55* (47), 6787–6790. https://doi.org/10.1039/C9CC02701G.

(80) Tranchemontagne, D. J.; Mendoza-Cortés, J. L.; O'Keeffe, M.; Yaghi, O. M. Secondary Building Units, Nets and Bonding in the Chemistry of Metal-Organic Frameworks. *Chem. Soc. Rev.* **2009**, *38* (5), 1257–1283. https://doi.org/10.1039/b817735j.

(81) Furukawa, H.; Kim, J.; Ockwig, N. W.; O'Keeffe, M.; Yaghi, O. M. Control of Vertex Geometry, Structure Dimensionality, Functionality, and Pore Metrics in the Reticular Synthesis of Crystalline Metal−Organic Frameworks and Polyhedra. *J. Am. Chem. Soc.* **2008**, *130* (35), 11650–11661. https://doi.org/10.1021/ja803783c.

(82) Comotti, A.; Bracco, S.; Ben, T.; Qiu, S.; Sozzani, P. Molecular Rotors in Porous Organic Frameworks. *Angew. Chem. Int. Ed.* **2014**, *53* (4), 1043–1047. https://doi.org/10.1002/anie.201309362.

(83) Khudozhitkov, A. E.; Jobic, H.; Kolokolov, D. I.; Freude, D.; Haase, J.; Stepanov, A. G. Probing the Guest-Mediated Structural Mobility in the UiO-66(Zr) Framework by ^{2}H NMR Spectroscopy. *J. Phys. Chem. C* **2017**, *121* (21), 11593–11600. https://doi.org/10.1021/acs.jpcc.7b03259.

(84) Vogelsberg, C. S.; Uribe-Romo, F. J.; Lipton, A. S.; Yang, S.; Houk, K. N.; Brown, S.; Garcia-Garibay, M. A. Ultrafast Rotation in an Amphidynamic Crystalline Metal Organic Framework. *Proc. Natl. Acad. Sci. USA* **2017**, *114* (52), 13613–13618. https://doi.org/10.1073/pnas.1708817115.

(85) Colin-Molina, A.; Jellen, M. J.; García-Quezada, E.; Cifuentes-Quintal, M. E.; Murillo, F.; Barroso, J.; Pérez-Estrada, S.; Toscano, R. A.; Merino, G.; Rodríguez-Molina, B. Origin of the Isotropic Motion in Crystalline Molecular Rotors with Carbazole Stators. *Chem. Sci.* **2019**, *10* (16), 4422–4429. https://doi.org/10.1039/C8SC04398A.

(86) Howe, M. E.; Garcia-Garibay, M. A. The Roles of Intrinsic Barriers and Crystal Fluidity in Determining the Dynamics of Crystalline Molecular Rotors and Molecular Machines. *J. Org. Chem.* **2019**, *84* (16), 9835–9849. https://doi.org/10.1021/acs.joc.9b00993.

(87) Deria, P.; Gomez-Gualdron, D. A.; Bury, W.; Schaef, H. T.; Wang, T. C.; Thallapally, P. K.; Sarjeant, A. A.; Snurr, R. Q.; Hupp, J. T.; Farha, O. K. Ultraporous, Water Stable, and Breathing Zirconium-Based Metal-Organic Frameworks with Ftw Topology. *J. Am. Chem. Soc.* **2015**, *137* (40), 13183–13190. https://doi.org/10.1021/jacs.5b08860.

(88) Parent, L. R.; Pham, C. H.; Patterson, J. P.; Denny, M. S.; Cohen, S. M.; Gianneschi, N. C.; Paesani, F. Pore Breathing of Metal-Organic Frameworks by Environmental Transmission Electron Microscopy. *J. Am. Chem. Soc.* **2017**, *139* (40), 13973–13976. https://doi.org/10.1021/jacs.7b06585.

(89) Souto, M.; Romero, J.; Calbo, J.; Vitorica-Yrezabal, I. J.; Zafra, J. L.; Casado, J.; Orti, E.; Walsh, A.; Minguez Espallargas, G. Breathing-Dependent Redox Activity in a Tetrathiafulvalene-Based Metal-Organic Framework. *J. Am. Chem. Soc.* **2018**, *140* (33), 10562–10569. https://doi.org/10.1021/jacs.8b05890.

SYNOPSIS TOC.